A LOW COST DRIVE FOR PERMANENT SPLIT CAPACITOR SINGLE PHASE INDUCTION MOTOR DRIVING A BLOWER

Luis C. Tomaselli, Denizar C. Martins and Ivo Barbi
UFSC – Universidade Federal de Santa Catarina
PGEEL – Programa de Pós Graduação em Engenharia Elétrica
INEP – Instituto de Eletrônica de Potência
lcandido@inep.ufsc.br; denizar@inep.ufsc.br; ivobarbi@inep.ufsc.br

***Abstract* – The goal of this paper is to propose a low cost adjustable speed drive for a permanent split capacitor (PSC) motor to drive a blower, using a relatively simple topology that establishes a reasonable compromise between energy savings and simplicity. The method employed in this study reduces the effective applied voltage, using a topology based on a three-phase inverter. The operating principle will be presented according to the theoretical statements, and experimental results obtained with a prototype driving a PSC motor validate the proposed analysis.**

KEYWORDS

PSC motor, chopper ac, fans, pumps, adjustable speed drive.

I. INTRODUCTION

The use of blowers in home appliances is very common. They are used for cooling, heating and circulation air systems. This paper proposes an electronic scheme to adjust the speed of a PSC motor driving a fan, where the main advantage lies in the continuous variable speed.

The method of adjusting the speed frequency is not suitable in this case. In a three-phase machine, the magnetizing current is maintained constant to avoid saturation so that a relation between voltage and frequency is set. In the PSC motor, there are two components of the magnetizing current. However, the relation between voltage and frequency is not as simple as in the case of the three-phase machine. Furthermore when the frequency decreases, the reactance increases, due to the capacitor in the auxiliary winding. This capacitor was designed for a nominal condition, and for different values this parameter needs to be modified [1]. Some authors have proposed the use of a two-phase converter but, due to the asymmetry of the PSC motor, different voltages must be applied to the main and auxiliary windings [2,3]. Usually the voltage on the auxiliary winding is higher than that on the main winding. If the relation between the voltages of the auxiliary and main windings is not maintained constant, the pulsating torques increase. For low frequencies, this is not a problem, because the value of the required voltage is low. However, for higher frequencies, this is not true, and it is necessary to use a converter to increase the value of the voltage, causing the cost to increase as well.

In this study, the method of reducing the effective applied voltage, keeping the synchronous speed, will be used. This causes the slip to increase and reduces the efficiency of the machine, although it is a simple way to obtain adjustable speed. It is adequate to say that the speed changes from about 50% to 100% if compared to the nominal value.

The most popular solution for speed control in blower applications is a PSC motor with taps. This paper proposes an electronic scheme to replace this system. The main advantage consists in the continuous variable speed.

Energy savings can be obtained with the scheme proposed, as explained below. Conceptually, a blower is a flux machine that transfers energy to air. It is obtained by means of a rotor and a wheel or, in other words, it sets the airflow into an ambient. Commonly in home appliances, they are of low-pressure type (specific energy lower than 500mmH_2O). In this situation, the blowers' third law is applicable. It states what occurs with pressure, airflow and power when the rotor speed changes (in this study, the air density is considered constant). The load power is proportional to the cube of the speed, while the airflow is proportional to the speed. It means that a little decrease in the speed leads to high reduction on the required load power.

Kragh [4] recommends a DC link regulator to obtain a variable AC sinusoidal output voltage. The power circuit consists of a unidirectional rectifier and a full-bridge inverter. Problems occur when the load current and voltage are not in the same quadrant. To deal with such problems, a bi-directional rectifier is used [5]. In this paper, a bi-directional rectifier and a half-bridge inverter are proposed.

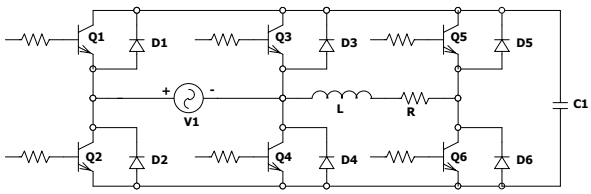

Fig. 1 – Proposed scheme.

II. DESCRIPTION OF THE CIRCUIT

The proposed circuit is presented in Fig. 1. Switches Q_1, Q_2, Q_3 and Q_4 constitute the bi-directional rectifier. Switches Q_1 and Q_4 are commutated to turn on and turn off in the positive and the negative semicycles, respectively. On the other hand, switches Q_2 and Q_3 are commanded to turn on and turn off in the negative and the positive semicycles, respectively. The inverter is composed of switches Q_5 and Q_6. They are switched in high frequency and in a complementary form. The capacitor at the DC link has a small value. For this reason, the voltage on the DC link is equal to the absolute value of the line voltage. The capacitor

is necessary due to a dead time. As the voltage on the DC link is the absolute value of a sinusoidal wave, the inverter circuit does not need a PWM sinusoidal modulation. However, it uses a PWM modulation to decrease the RMS value of the load voltage. Switch Q_5 conducts in the positive semicycle and Q_6 in the negative one.

Due to intrinsic symmetry, only the positive semicycle will be analyzed. During this interval, switches Q_1 and Q_4 are conducting and Q_2 and Q_3 are blocked. Switches Q_5 and Q_6 are commanded in a complementary form and their driver signals are provided in Fig. 2.

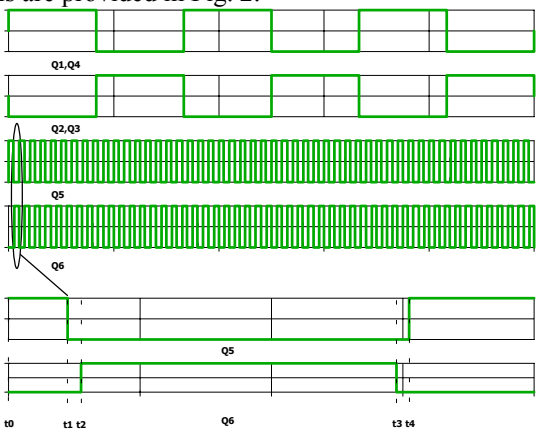

Fig. 2 – Driver signals of the rectifier and inverter cicruits.

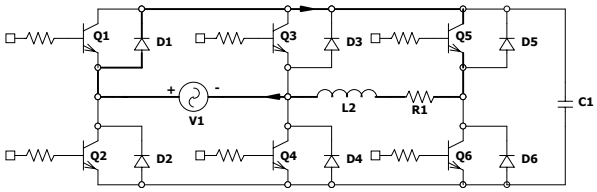

Fig. 3 – Stage 1 (first case).

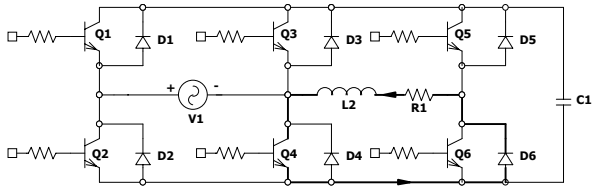

Fig. 4 – Stages 2 to 4 (first case).

In the mathematical analysis, the PSC motor is treated as an inductive load. Two cases are possible. In the first one, the load current and voltage are not in the same quadrant. In the second one, both them are in the same quadrant. According to the respective quadrants, the following analysis is carried out.

A. First case – load current and voltage in the same quadrant.

Stage 1 (t_0-t_1) – this interval begins at t_0, when switches Q_1 and Q_4 are conducting. Switches Q_2 and Q_3 are blocked. Switch Q_5 is conducting, and therefore Q_6 is blocked. During this interval, the energy flows from the input source to the load. The interval finishes at t_1, when Q_5 is turned off (Fig. 3).

Stage 2 (t_1-t_2) – during this interval, the load current flows through Q_4 and D_6. This interval corresponds to a dead time (Fig. 4).

Stage 3 (t_2-t_3) – at instant t_2, Q_6 is turned on and Q_5 is turned off. The load current flows through Q_4 and D_6 (Fig. 4).

Stage 4 (t_3-t_4) – at instant t_3, Q_6 is blocked. The load current keeps flowing through Q_4 and D_6 (Fig. 4). This is equivalent to a dead time interval (Fig. 4).

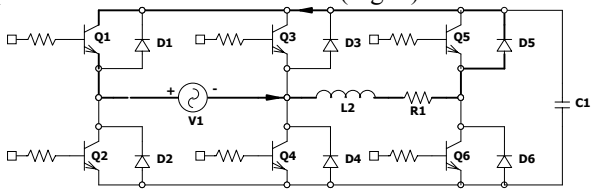

Fig. 5 – Stage 1, 2 and 4 (second case).

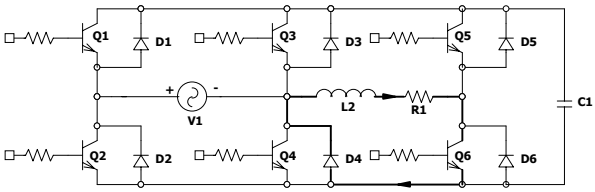

Fig. 6 – Stage 3 (second case).

B. Second case – load current and voltage in different quadrant.

Stage 1 (t_0-t_1) – this interval begins at t_0, when switches Q_1 and Q_4 are turned on. Switches Q_2 and Q_3 are blocked, and Q_5 is turned on while Q_6 is blocked. During this interval, the energy flows from the load to the input source. The interval finishes at t_1, when Q_5 is tuned off. During this interval, the load current flows through Q_1 and D_5 (Fig. 5).

Stage 2 (t_1-t_2) – during this interval, the load current flows through Q_1 and D_5. This corresponds to a dead time interval (Fig. 5).

Stage 3 (t_2-t_3) – at instant t_2, switch Q_6 is turned on and Q_5 is turned off. The load current flows through Q_6 and D_4 (**Fig. 6**).

Stage (t_3-t_4) – at instant t_3, switch Q_6 is turned off. The load current flows through Q_1 and D_5. This is equivalent to a dead time interval (Fig. 5).

C. Output Voltage and Output Current

The output voltage is equal to the input voltage multiplied by the switching function. Therefore the output voltage is given by (1).

$$v_s(t) = \sqrt{2} \cdot D \cdot V_{rms} \sin(\omega_r t) + \sum_{k=1}^{\infty} \sqrt{2} \frac{V_{rms} \sin(kD\pi)}{k\pi} \cdot \sin(k\omega_s t) \quad (1)$$

It is composed by a fundamental term plus a harmonic content. The RMS value of the output voltage is stated by (2).

$$V_{s(rms)} = V_{in(rms)} \sqrt{D} \quad (2)$$

The load impedance is defined by (3):

$$Z(s) = R + sL \quad (3)$$

The load impedance works as a filter so that the harmonic magnitudes of the load current are low. In steady state, the

RMS value of the load current is given by (4):

$$I_{c(rms)} = \frac{V_{rms}}{\sqrt{R^2 + \omega_r{}^2 L^2}} \cdot D \quad (4)$$

while the RMS value of the load current harmonics is given by (5):

$$I_{c(rms)} = \frac{\sqrt{2} \cdot V_{rms} \sin(kD\pi)}{k\pi \sqrt{R^2 + k^2 \omega_s{}^2 L^2}} \quad (5)$$

The total harmonic distortion (THD) of the load current is specified by:

$$THD_{Io}(D) = 100 \frac{\sqrt{\sum_{k=1}^{\infty} \frac{\sqrt{2} \cdot \sin(kD\pi)}{k\pi \sqrt{R^2 + k^2 \omega_s{}^2 L^2}}}}{\frac{D}{\sqrt{R^2 + \omega_r{}^2 L^2}}} \quad (6)$$

From (6), it can be noticed that the THD will be low due to the switching frequency. Therefore, the load current harmonics will not be considered in the next steps.

D. Input Current

The load current is defined by (7).

$$i_c(t) = \frac{\sqrt{2} \cdot V_{rms}}{\sqrt{R^2 + \omega_r{}^2 L^2}} \cdot D \cdot \sin\left(\omega_r t - \tan^{-1}\left(\frac{\omega_r L}{R}\right)\right) \quad (7)$$

The input current is equal to the load current multiplied by the switching function. Therefore the input current is given by (8).

$$i_{in}(t) = I_p \cdot D^2 \cdot \sin(\omega_r t - \phi) + \\ + \sum_{k=1}^{\infty} \frac{D \cdot I_p \sin(kD\pi)}{k\pi} \cdot \sin(k\omega_s t \pm (\omega_r t - \phi)) \quad (8)$$

The THD of the input current is stated by (9).

$$THD_{Iin}(D) = 100 \frac{\sqrt{\sum_{k=1}^{\infty} 2\left(\frac{\sin(kD\pi)}{k\pi}\right)^2}}{D} \quad (9)$$

One can notice that the THD_{Iin} is a function of the duty cycle only. Harmonics appear around the switching frequency, as it is quite simple to filter them.

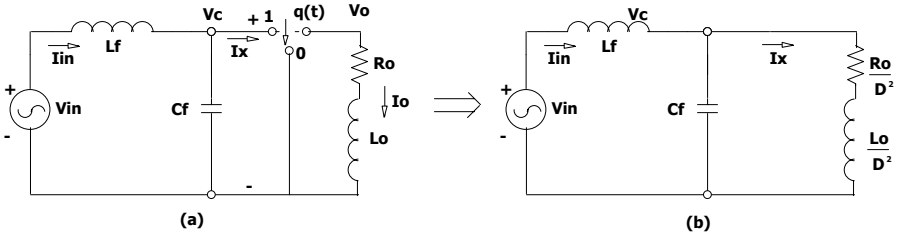

Fig. 7 – Equivalent circuit for the converter with the LC filter.

E. Input Filter

The input current is pulsed and a LC filter will be used here. Moreover there is a displacement between the fundamental input current and voltage. The LC filter will be specified to decrease the THD_{Iin} and the displacement.

Equivalents circuits for the converter are shown in Fig. 7. Fig. 7(a) presents the converter while Fig. 7(b) depicts the converters' averaged model. From Fig. 7(b) expression (10) is obtained.

$$\frac{Iin(j\omega_r)}{Vin(j\omega_r)} = \frac{D^2 - \omega_r{}^2 L_0 C_f + j\omega_r C_f R_0}{R_0 - \omega_r{}^2 C_f L_f R_0 + j\omega_r \left(L_0 + L_f D^2 - \omega_r{}^2 L_f L_0 C_f\right)} \quad (10)$$

If the phase is set to zero in (10), the filter inductance L_f can be determined by (11).

$$L_f = \frac{L_0 D^2 - C_f \left(\omega_r{}^2 L_0{}^2 + R_0{}^2\right)}{2\omega_r{}^2 C_f L_0 D^2 - \omega_r{}^2 C_f{}^2 \left(R_0{}^2 + \omega_r{}^2 L_0{}^2\right) - D^4} \quad (11)$$

Expression (11) shows that the filter inductance is a function of the load, the capacitance of the filter and the duty cycle. Other factor that influences the filter parameters is the resonance frequency. From the resonance frequency, the filter capacitance is determined as a function of the filter inductance, which is then determined by (12).

$$L_{f1,2} = \frac{200\omega_r{}^2 L_0 - L_0 \omega_s{}^2 \pm \sqrt{L_0{}^2 \omega_s{}^4 + \left(400\omega_s{}^2 - 40000\omega_r{}^2\right) R_0{}^2}}{2\omega_s{}^2 \cdot D^2} \quad (12)$$

Hence, the filter capacitance is determined using (13).

$$C_f = \frac{100}{L_f \cdot \omega_s{}^2} \quad (13)$$

The THD_{Iin} is given by (14).

$$DHT_{Iin}(D) = 100 \frac{\sqrt{\sum_{k=1}^{\infty} 2\left(\frac{\text{sen}(kD\pi)}{k\pi}\right)^2 \cdot \left(\frac{1}{1+100 \cdot k^2}\right)}}{D} \quad (14)$$

III. Design and Simulation Results

A. Design Procedure

Simulation results and a design example of the studied converter are presented in this section. A simplified design procedure to calculate some of the components is used. The specifications are as follows:

Vin_{pk} = 311V, I_0 = 0.38A, f_r = 60Hz, f_{sw} = 20kHz,

L_{eq} = 0.216H and R_{eq} = 516Ω.

Using (12) and (13), it provides the values given by (15)

and (16).

$$L_f = 7,7mH \quad (15)$$

$$C_f = 820nF \quad (16)$$

The THD of the input current without the filter is presented in Fig. 8. The THD of the output current is shown in the Fig. 9.

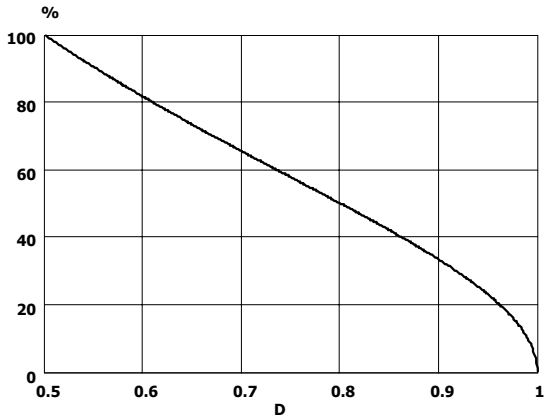

Fig. 8 – Input current THD as a function of the duty cycle.

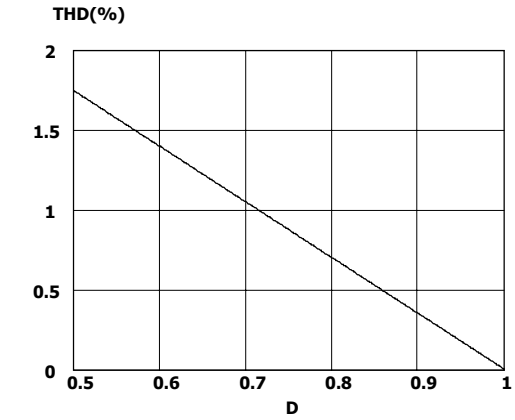

Fig. 9 – Output current THD as a function of the duty cycle.

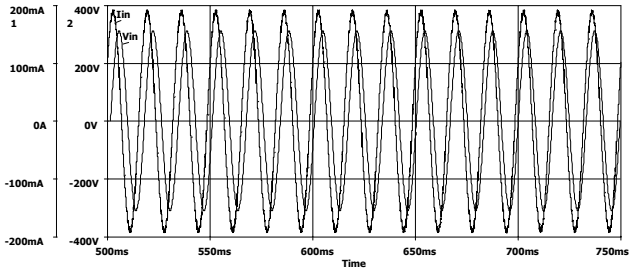

Fig. 10 – Input current (134mArms) and voltage of the converter driving a PSC motor with D = 0,5.

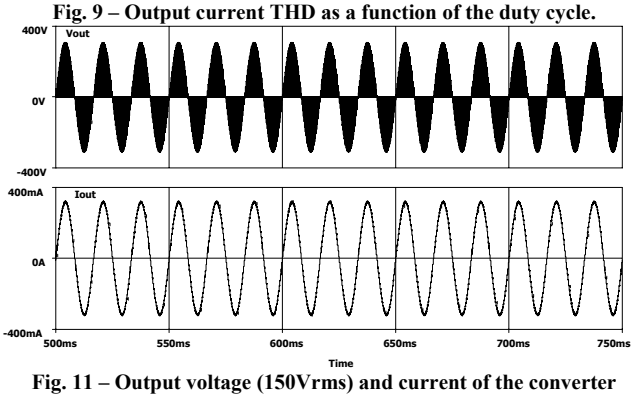

Fig. 11 – Output voltage (150Vrms) and current of the converter driving a PSC motor with D = 0,5.

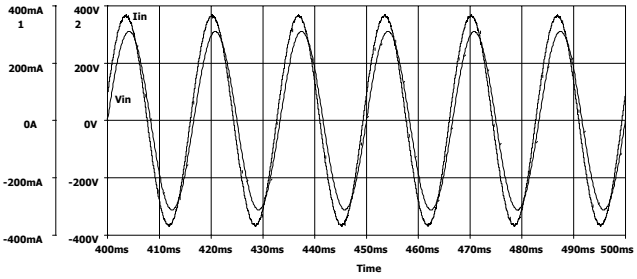

Fig. 12 – Input current (259mArms) and voltage of the converter driving a PSC motor with D = 0,75.

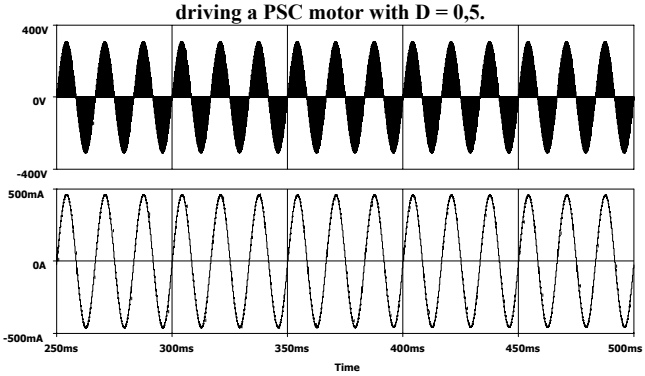

Fig. 13 – Output voltage (189Vrms) and current of the converter driving a PSC motor with D = 0,75.

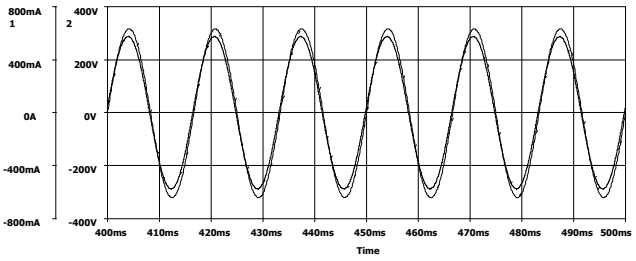

Fig. 14 – Input current (400mArms) and voltage of the converter driving a PSC motor with D = 1.

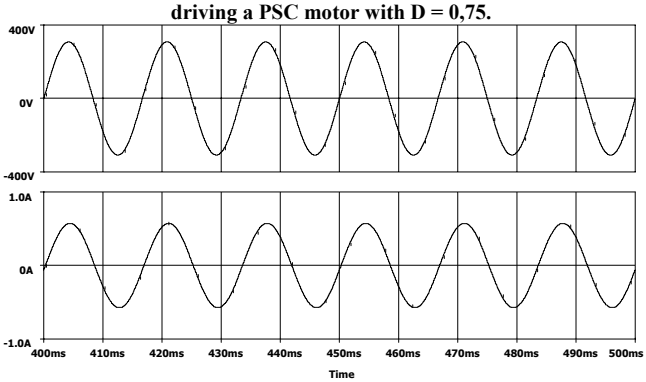

Fig. 15 – Output voltage (220Vrms) and current of the converter driving a PSC motor with D = 1.

B. Simulation results

In this section, the operating waveforms of the proposed converter driving a PSC motor in steady state obtained by simulation analysis are presented. The PSC motor characteristics are as follows, 4 poles (2 pairs of poles), 80W, 60Hz and 220V.

The electrical parameters of the motor and the load torque characteristic were obtained by experimental tests.

The simulation tests of the proposed converter were performed using different values of duty cycle. The machine was modeled using dq transform in stator reference frame [6,7,8].

The first simulation was performed using D=0.5. Fig. 10 presents the input current and voltage obtained by simulation. The simulation results show that the high harmonics content and the displacement factor were adjusted. Fig. 11 shows the output current and voltage. As expected, the load current is higher than the input current. Fig. 12 presents the simulation results concerning the input current (after filtering) and the input voltage with D=0.75. Fig. 13 shows the output current and voltage with D=0.75. Finally, Fig. 14 presents the input current and voltage for D=1. One can see that the displacement is null in this situation (nominal case). Fig. 15 shows the output voltage and current for this case.

Under the conditions stated above, it can be seen that the RMS value of the output voltage can be controlled by means of the duty cycle, as well as the speed of the motor. Sinusoidal input and output current waveform can be obtained with high power factor.

IV. Experimental Results

The proposed converter was designed and tested in laboratory. The same operating conditions presented in simulation results were performed for the prototype.

The experimental waveforms of the proposed converter are shown in Fig. 16 to Fig. 21. In Fig. 16, Fig. 18 and Fig. 20, the input current and voltage waveforms are presented for different values of duty cycle. One can notice that the input current waveform is sinusoidal as desired.

Fig. 17 shows the output voltage when D = 0.75, where it can be noticed that the waveform is sinusoidal. In Fig. 19, the output current with D = 0.75 is presented.

Fig. 21 shows the input current in the transient time. The current does not have a high value during the transient time due to high value of the stator winding resistance.

TABLE I
Experimental results for the converter driving the PSC motor

D	Input Power (W)	Speed (rpm)
0,5	23	538
0,6	33	663
0,7	44	775
0,8	56	890
0,9	63	998
1	79	1116

Table 1 presents some experimental results. From this table, it can be noticed that the speed is proportional to the duty cycle. It occurs because the torque is proportional to the square of the output voltage, and the output voltage is proportional to the square root of the duty cycle. As expected, the input power is proportional to the cube of the variation on the duty cycle.

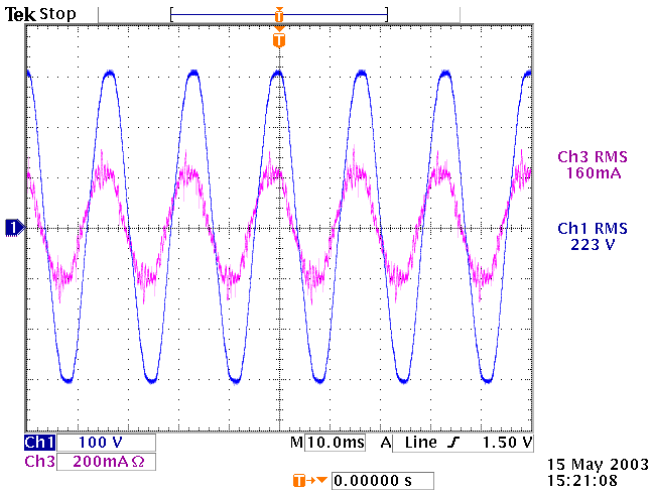

Fig. 16 – Input voltage and current of the converter for D = 0,5.

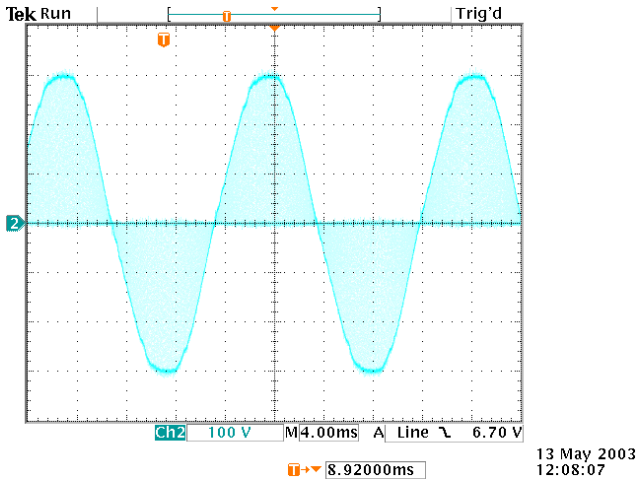

Fig. 17 – Output voltage of the converter for D = 0,75.

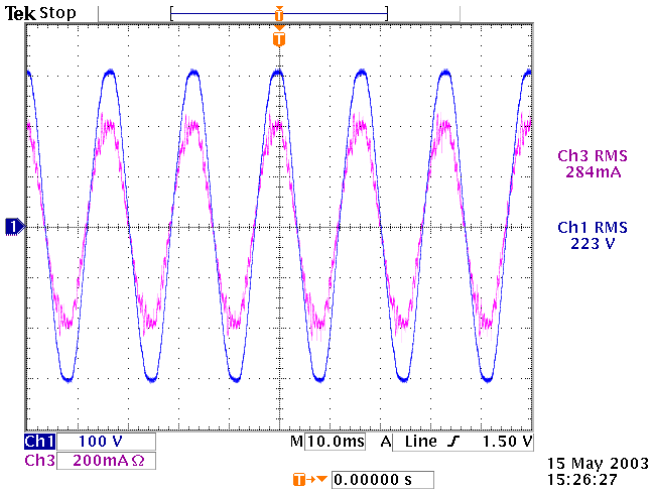

Fig. 18 – Input voltage and current of the converter for D = 0,75.

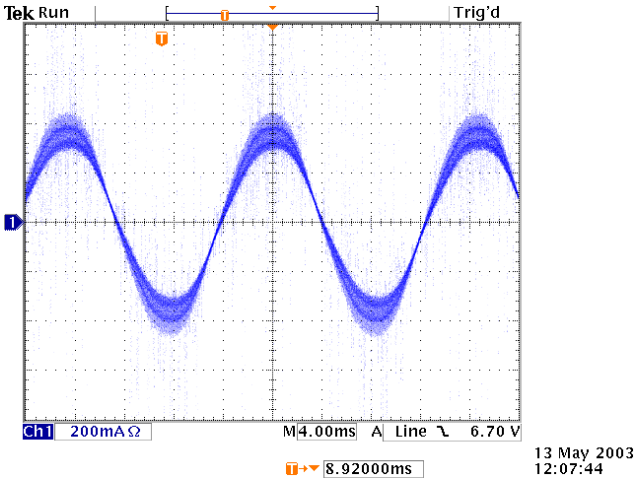

Fig. 19 – Output current of the converter for D = 0,75.

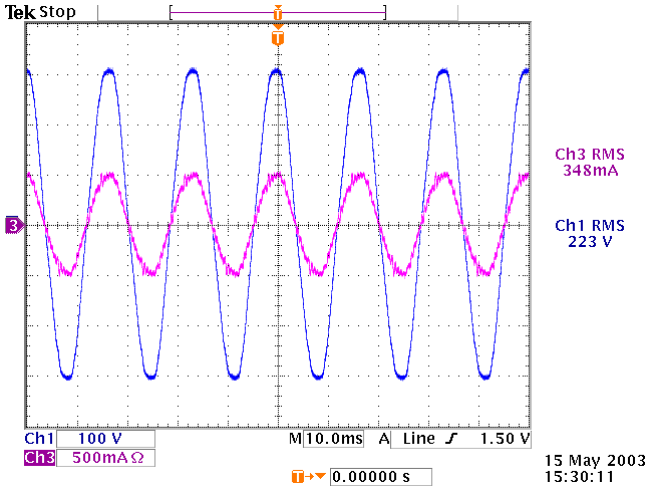

Fig. 20 – Input voltage and current of the converter for D = 1.

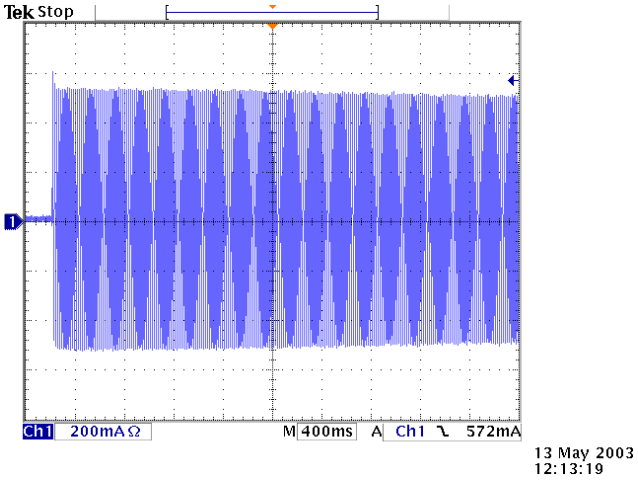

Fig. 21 – Transient of the Input current of the converter for D = 1.

V. CONCLUSION

In this paper, a simple and low cost speed drive for a PSC motor was presented, which can be used for blower applications. This converter can be used in applications that demands a sinusoidal voltage lower than the input voltage, and where the load current does not need to be in phase. The inverter circuit does not need a sinusoidal PWM modulation due to the small capacitance employed in the DC link. The LC filter was designed in order to eliminate the harmonic content and correct the displacement factor.

ACKNOWLEDGEMENT

The authors acknowledge the contribution of CNPq by the financial support.

REFERENCES

[1] T. M. Lettenmaier, D. W. Novotny, T. A. Lipo. "Single phase induction motor with an electronically controlled capacitor." *Industry Applications Society Annual Meeting, 1988. Conference Record of the 1988*. IEEE 1988. Vol. 1 pp 169-174.

[2] C. Young, C. Liu. "New Inverter Driven Design and Control Method for Two-Phase Induction Motor Drives." *IEE Proceedings on Electric Power Application*, Vol. 143, Nº 6, November 2996, pp. 458-466.

[3] D. G. Holmes and A. Kotsopoulos. "Variable Speed Control of Single and Two Phase Induction Motors using a Three Phase Induction Motors using a Three Phase Voltage Source Inverter." *Proceedings of IEE Conference*, 1993, pp. 613-620.

[4] Kragh, H.. "On the control of a dc-link high frequency ac-voltage regulator". *IEEE*. 2001.

[5] Kwon, B.H., Jeong, G.Y., Hah, S.H. And Lee, D.H. "Novel Line conditioner with Voltage Up/Down Capability". *IEEE Transactions on Industrial Electronics*, Vol. 49, Nº, 5, October 2002. 1110-1118p.

[6] Krause, P. C.. "Analysis of Electric Machinery". *2. ed. New York: Ed. McGraw-Hill*, 1986. 564p.

[7] Barbi, I.. "Teoria Fundamental do Motor de Indução". 1. ed. Florianópolis: *Ed. da UFSC*, 1985. 237p.

[8] Jones, C. V.. "The Unified Theory of Electrical Machines". Belfast: *Ed. Butterworths*, 1967. 542p.